CORRIGENDUM

ALEXEY YU. KARPECHKO AND NATHAN P. GILLETT

Climatic Research Unit, School of Environmental Sciences, University of East Anglia, Norwich, East Anglia, United Kingdom

GARETH J. MARSHALL

British Antarctic Survey, Cambridge, United Kingdom

JAMES A. SCREEN

Climatic Research Unit, School of Environmental Sciences, University of East Anglia, Norwich, East Anglia, United Kingdom

In Karpechko et al. (2009), the two Screen et al. references were set and thus cited incorrectly. The correct citations are as below:

The influence of the SAM has also been identified in moisture transport and precipitation (Boer et al. 2001), storm track activity and regional rainfall (Brahmananda Rao et al. 2003), sea surface temperature (Mo 2000; Hall and Visbeck 2002; Screen et al. 2009b), ocean circulation (Hall and Visbeck 2002; Sen Gupta and England 2006, hereafter referred to as SGE06), and sea ice concentration (Lefebvre et al. 2004; Liu et al. 2004).

Screen et al. (2009b) also showed that model resolution does not strongly impact the short-term SST response to the SAM in an ocean model run at various horizontal resolutions.

Screen et al. (2009a) showed that the observed negative SST response over the Pacific is associated with negative anomalies in the observed atmosphere-to-ocean heat fluxes, and the observed positive SST response east of Drake Passage is associated with positive anomalies in atmosphere-to-ocean heat fluxes. They suggest that the observed atmosphere-to-ocean heat flux anomalies in these regions are associated with observed zonal asymmetry in the SLP response, which is not simulated by the models.

However, Screen et al. (2009a), studying the initial SST response to the SAM, show that in most of the Southern Ocean the ocean–atmosphere heat fluxes are associated with SATO anomalies driving SST anomalies rather than the other way round.

Screen et al. (2009a) analyzed the SAM responses in four CMIP3 models and found that in their subset all of the models simulated a too-strong anomalous Ekman flow related to a too-strong zonal wind response. They concluded that the errors in the simulated Ekman heat flux are larger than the other mixed layer heat budget terms over most latitudes within 40°–65°S. North of 40°S, errors in the atmosphere-to-ocean heat fluxes become increasingly important.

This is confirmed by Screen et al. (2009a) who performed a detailed study of the terms of the ocean mixed layer heat budget.

While the simulations only possess limited skill in representing the short-term SST response to the SAM, the long-term response, which is influenced by mesoscale eddies, may be even more questionable (i.e., Screen et al. 2009b).

The staff of the *Journal of Climate* regrets any inconvenience this error may have caused.

REFERENCES

Boer, G. J., S. Fourest, and B. Yu, 2001: The signature of the annular modes in the moisture budget. *J. Climate,* **14,** 3655–3665.

Brahmananda Rao, V., A. M. C. do Carmo, and S. Franchito, 2003: Interannual variations of storm tracks in the Southern Hemisphere and their connections with the Antarctic Oscillation. *Int. J. Climatol.,* **23,** 1537–1545.

Hall, A., and M. Visbeck, 2002: Synchronous variability in the Southern Hemisphere atmosphere, sea ice, and ocean resulting from the annular mode. *J. Climate,* **15,** 3043–3057.

Karpechko, A. Yu., N. P. Gillett, G. J. Marshall, and J. A. Screen, 2009: Climate impacts of the southern annular mode simulated by the CMIP3 models. *J. Climate,* **22,** 3751–3768.

Corresponding author address: Alexey Karpechko, Climatic Research Unit, School of Environmental Sciences, University of East Anglia, NR4 7TJ, Norwich, United Kingdom.
E-mail: a.karpechko@uea.ac.uk

DOI: 10.1175/2009JCLI3400.1

Lefebvre, W., H. Goosse, R. Timmermann, and T. Fichefet, 2004: Influence of the Southern Annular Mode on the sea ice–ocean system. *J. Geophys. Res.,* **109,** C09005, doi:10.1029/2004JC002403.

Liu, J., J. A. Curry, and D. G. Martinson, 2004: Interpretation of recent Antarctic sea ice variability. *Geophys. Res. Lett.,* **31,** L02205, doi:10.1029/2003GL018732.

Mo, K. C., 2000: Relationships between low-frequency variability in the Southern Hemisphere and sea surface temperature anomalies. *J. Climate,* **13,** 3599–3610.

Screen, J. A., N. P. Gillett, A. Yu. Karpechko, and D. P. Stevens, 2009a: Mixed layer temperature response to the southern annular mode: Mechanisms and model representation. *J. Climate,* in press.

——, ——, D. P. Stevens, G. J. Marshall, and H. K. Roscoe, 2009b: The role of eddies in the Southern Ocean temperature response to the southern annular mode. *J. Climate,* **22,** 806–818.

Sen Gupta, A., and M. H. England, 2006: Coupled ocean–atmosphere–ice response to variations in the southern annular mode. *J. Climate,* **19,** 4457–4486.

Climate Impacts of the Southern Annular Mode Simulated by the CMIP3 Models

ALEXEY YU. KARPECHKO AND NATHAN P. GILLETT

Climatic Research Unit, School of Environmental Sciences, University of East Anglia, Norwich, East Anglia, United Kingdom

GARETH J. MARSHALL

British Antarctic Survey, Cambridge, United Kingdom

JAMES A. SCREEN

Climatic Research Unit, School of Environmental Sciences, University of East Anglia, Norwich, East Anglia, United Kingdom

(Manuscript received 13 August 2008, in final form 16 December 2008)

ABSTRACT

The southern annular mode (SAM) has a well-established impact on climate in the Southern Hemisphere. The strongest response in surface air temperature (SAT) is observed in the Antarctic, but the SAM's area of influence extends much farther, with statistically significant effects on temperature and precipitation being detected as far north as 20°S. Here the authors quantify the ability of the Coupled Model Intercomparison Project, phase 3 (CMIP3) coupled climate models to simulate the observed SAT, total precipitation, sea surface temperature (SST), and sea ice concentration responses to the SAM. The models are able to simulate the spatial pattern of response in SAT reasonably well; however, all models underestimate the magnitude of the response over Antarctica, both at the surface and in the free troposphere. This underestimation of the temperature response has implications for prediction of the future temperature changes associated with expected changes in the SAM. The models possess reasonable skill in simulating patterns of precipitation and SST response; however, some considerable regional deviations exist. The simulated precipitation and SST responses are less constrained by the observations than the SAT response, particularly in magnitude, as significant discrepancies are detected between the responses in the reference datasets. The largest problems are identified in simulating the sea ice response to the SAM, with some models even simulating a response that is negatively correlated with that observed.

1. Introduction

The variability of the Southern Hemispheric extratropical circulation is dominated by the large-scale southern annular mode (SAM), which explains about 27% of the total hemispheric 850-hPa geopotential height variance south of 20°S (Thompson and Wallace 2000). This mode is essentially zonally symmetric, equivalent barotropic, and characterized by sea level pressure (SLP) and geopotential height anomalies in high and midlatitudes of opposite sign, with the node at about 55°S. The positive phase of the SAM is associated with anomalously low pressure over high latitudes. The anomalies in air mass distribution are accompanied by changes in the strength and position of the midlatitude westerlies. During the positive phase of the SAM the westerlies move poleward and strengthen, while in the negative phase they move equatorward and weaken.

A number of SAM definitions are used in the literature. Thompson and Wallace (2000) defined the SAM as the leading empirical orthogonal function (EOF) of geopotential height variability at the 850-hPa pressure surface, although the first EOF of SLP (Miller et al. 2006; Cai and Cowan 2007) and geopotential height at the 500-hPa pressure surface (e.g., Cai and Watterson 2002 and references therein) have also been used. An alternative definition was suggested by Gong and Wang (1999) who defined the SAM (referred to as the Antarctic Oscillation) as a difference between the zonal mean SLP at 40° and 65°S. Marshall (2003) used this latter definition to calculate the SAM index using SLP

Corresponding author address: Alexey Karpechko, Climatic Research Unit, School of Environmental Sciences, University of East Anglia, NR4 7TJ, Norwich, United Kingdom.
E-mail: a.karpechko@uea.ac.uk

DOI: 10.1175/2009JCLI2788.1

from 12 stations, 6 each along the aforementioned latitudes.

The SAM has a profound effect on Antarctic climate (Thompson and Wallace 2000; Marshall 2007). During the positive phase the Antarctic continent cools as a result of anomalous upwelling and associated adiabatic cooling. In some regions, the background cooling is enhanced by decreased meridional heat transport from the warmer ocean and decreased vertical turbulent heat transport from the free troposphere due to a weakening of surface-layer winds and an associated weakening of turbulent mixing (van den Broeke and van Lipzig 2003). At the same time the Antarctic Peninsula warms as a result of fewer cold air outbreaks from the continent and intensified advection of warm air from the ocean. The influence of the SAM has also been identified in moisture transport and precipitation (Boer et al. 2001), storm track activity and regional rainfall (Brahmananda Rao et al. 2003), sea surface temperature (Mo 2000; Hall and Visbeck 2002; Screen et al. 2009), ocean circulation (Hall and Visbeck 2002; Sen Gupta and England 2006, hereafter referred to as SGE06), and sea ice concentration (Lefebvre et al. 2004; Liu et al. 2004).

The impact of the SAM on climate extends beyond Antarctica and is identifiable as far north as 20°S (e.g., Gillett et al. 2006). Several regional studies have detected a SAM influence on precipitation over southeastern South America (Silvesteri and Vera 2003), South Africa (Reason and Rouault 2005), Australia (Cai et al. 2005; Hendon et al. 2007; Meneghini et al. 2007), and New Zealand (Renwick and Thompson 2006). Some of these studies have pointed out considerable seasonality in the impact of the SAM.

During recent decades the SAM index has exhibited a trend toward positive values (see Marshall 2003 and references therein), which is likely due to a combination of ozone depletion and greenhouse gas increases (Gillett and Thompson 2003; Marshall et al. 2004; Shindell and Schmidt 2004; Arblaster and Meehl 2006). It has been shown that this trend contributed to observed decreases in Australian rainfall (e.g., Li et al. 2005) and Antarctic surface temperature changes (Thompson and Solomon 2002; Kwok and Comiso 2002; Marshall et al. 2006; Chapman and Walsh 2007; Marshall 2007). Simulations of future climate with atmosphere–ocean general circulation models (AOGCMs) suggest that the SAM index will continue to increase as a response to projected increases in greenhouse gas concentrations (Shindell and Schmidt 2004; Miller et al. 2006). However, some AOGCMs that account for the expected ozone recovery simulate a decrease of the SAM index during austral summer (Perlwitz et al. 2008; Son et al. 2008). Models containing interactive atmospheric chemistry and, in general, a better representation of the stratosphere also simulate the summer SAM index decrease (Perlwitz et al. 2008; Son et al. 2008). Irrespective of the direction of the future SAM trend, any changes in the SAM would be expected to influence the Southern Hemisphere climate. The question, which we address, is how well are climate models able to simulate the climate impacts of the SAM?

Qualitative agreement between simulated and observed signatures of the SAM on atmospheric and ocean variables has been demonstrated for individual models by several authors (Watterson 2000; Hall and Visbeck 2002; Cai and Watterson 2002; SGE06; Cai and Cowan 2006; Watterson 2007). However, none of these studies provided a quantitative assessment across multiple models. In this study we quantify the ability of the Coupled Model Intercomparison Project phase 3 (CMIP3) models used in the Intergovernmental Panel on Climate Change (IPCC) Fourth Assessment Report (AR4) to simulate the impact of the SAM on surface air temperature (SAT), precipitation (PRE), sea surface temperature (SST), and sea ice concentration (SIC). The ability of CMIP3 models to simulate different aspects of Antarctic climate has been assessed in several studies using a subset of the CMIP3 models. Miller et al. (2006), Raphael and Holland (2006), and Cai and Cowan (2007), using SLP and the 850-hPa geopotential height fields, showed that the models simulate a realistic SAM pattern; Parkinson et al. (2006) and Holland and Raphael (2006) showed that the models reproduce the observed seasonality of Antarctic sea ice reasonably well, although some models simulate either too much or too little ice; Russell et al. (2006) demonstrated that all models but one reveal considerable deficiency in simulating the strength and position of the Antarctic Circumpolar Current; while Connolley and Bracegirdle (2007) created a metric that combined model errors in simulating several Antarctic and global climate variables to quantify the overall skill of a model in simulating Antarctic climate.

2. Data and methods

Model data were retrieved from the CMIP3 dataset (available online at http://www-pcmdi.llnl.gov/). For both Goddard Institute for Space Studies Model E (GISS-E) models data was downloaded directly from the GISS server (ftp://data.giss.nasa.gov/pub/pcmdi/). Table 1 lists the models used for this study. Altogether, data from 24 models are used for all variables except for

TABLE 1. CMIP3 model names and number of simulations used in this study.

Model name and country	*N* runs used		
	Air	SST	SIC
BCCR BCM2.0, Norway	1	1	1
Canadian Centre for Climate Modelling and Analysis (CCCma) Coupled General Circulation Model, version 3.1 CGCM3.1 T47, Canada	5	4	5
CCCma CGCM3.1 T63, Canada	1	1	1
Centre National de Recherches Météorologiques Coupled Global Climate Model, version 3(CNRM-CM3), France	1	1	1
CSIRO Mk3.0, Australia	3	2	3
CSIRO Mk3.5, Australia	1	1	1
Geophysical Fluid Dynamics Laboratory Climate Model version 2.0 (GFDL CM2.0), United States	3	3	3
GFDL CM2.1, United States	3	3	3
GISS-ER, United States	5	5	5
GISS-EH, United States	5	5	—
GISS-AOM, United States	2	2	2
FGOALS-g1.0, China	3	1	—
INGV-SXG, Italy	1	1	1
INM-CM3.0, Russia	1	1	1
IPSL CM4, France	2	1	1
MIROC3.2(hires), Japan	1	1	—
MIROC3.2(medres), Japan	3	1	3
ECHAM5/Max Planck Institute Ocean Model (MPI-OM), Germany	4	3	3
ECHAM and the global Hamburg Ocean Primitive Equation (ECHO-G), Germany/South Korea	5	3	3
MRI CGCM2.3.2, Japan	5	5	5
Community Climate System Model, version 3.0 (CCSM3.0), United States	8	2	5
PCM, United States	4	3	—
UKMO HadGEM1, United Kingdom	2	2	2
UKMO HadCM3, United Kingdom	2	2	2

sea ice. For the latter, data from Flexible Global Ocean–Atmosphere–Land System Model gridpoint version 1.0 (FGOALS-g1.0), GISS-EH, Parallel Climate Model (PCM), and Model for Interdisciplinary Research on Climate 3.2, high-resolution version [MIROC3.2(hires)] are excluded from the analysis. FGOALS-g1.0 shows much more extensive sea ice than the observations (Connolley and Bracegirdle 2007), while GISS-EH has sea ice extending over the Antarctic continent, perhaps owing to an error in postprocessing or data storage. PCM and MIROC3.2(hires) have too many missing values. The total number of available simulations (including multiple realizations for some models) varies between 71 for SAT and PRE and 51 for SIC.

Several sources of observational data are used here to validate the models. SLP and SAT are taken from the 40-yr European Centre for Medium-Range Weather Forecasts (ECMWF) Re-Analysis (ERA-40) (Uppala et al. 2005). PRE is taken from the Global Precipitation Climatology Project, version 2 (GPCP) (Adler et al. 2003). GPCP is a merged analysis that incorporates surface rain gauge observations and satellite precipitation estimates based on microwave and infrared data. SST and SIC are taken from the Hadley Centre Sea Ice and Sea Surface Temperature dataset (HadISST) (Rayner et al. 2003). Additionally, SAT and SLP fields from the National Centers for Environmental Prediction/Department of Energy Atmospheric Model Intercomparison Project II reanalysis (NR2) (Kanamitsu et al. 2002) and SST from the NOAA Optimum Interpolation Sea Surface Temperature V2 (NOAA OI SST) (Reynolds et al. 2002) dataset are used to estimate the possible impact of the choice of reference datasets. For PRE, the two reanalyses datasets (ERA-40 and NR2) and also Climate Prediction Center (CPC) Merged Analysis of Precipitation (CMAP) (Xie and Arkin 1997) are used. In general, the use of reanalysis products for model validation is justified because we use only data from the satellite period when the observational coverage is good and therefore monthly variability, which we are interested in, is expected to be captured well.

The station-based SAM index used in this study is described in Marshall (2003) with some modifications as described below. For uniformity of the analysis, the SAM in reanalyses and models was defined similarly and calculated by interpolating original SLP to the coordinates of stations used in Marshall (2003). Marshall

et al. (2004) employed the same approach and showed that the correlation with an EOF-based index is very high ($r = 0.98$). Note that higher variability should be expected for a station-based SAM index, compared to an EOF-based or zonal mean index, due to contributions from small-scale processes. Additional tests show that the results of the study are not sensitive the choice of index definition. Screen et al. (2009) also showed that model resolution does not strongly impact the short-term SST response to the SAM in an ocean model run at various horizontal resolutions.

The impacts of the SAM are estimated by regressing detrended monthly mean climate anomalies on a detrended monthly mean SAM index. Linear trends are calculated for each month separately. Because SAM variability may differ between datasets, we do not normalize the SAM index but simply subtract mean SLP at the stations at 65°S from mean SLP at the stations at 40°S. Thus, the index is in pressure units. Before regression, the atmospheric data are interpolated onto a 5° × 5° grid, which is the approximate resolution of the coarsest model (GISS-E). Although the coarsest oceanic model (GISS-ER) has a resolution of 4° × 5°, the oceanic data are interpolated onto a 2° × 2° grid. This is done because the majority of the datasets have a resolution higher than 2° × 2°. We found that the interpolation grid size has no strong impact on the results.

The regression pattern for an individual model is obtained by averaging over the regression patterns for all realizations available for that model. Averaging across all models (i.e., giving equal weight to each model) gives the multimodel response (MULTI). The alternative averaging, for which equal weight is given to each realization rather than to each model, gives similar results.

Owing to possible problems in the presatellite reanalysis data, we restrict our attention to the period of 1979–2001 for the atmospheric data and 1982–2007 for the oceanic data. GPCP precipitation is available for the period of 1979–2007. To keep the same length of time series as in observations and since many simulations finish in 1999, we use model SLP and SAT from the period 1977–99, PRE from the period 1971–99, and model oceanic data from the period 1974–99 in the twentieth-century simulations of each model. Since the data are detrended prior to the analysis, the small differences in periods between models and observations are not expected to influence the results.

As a tool to compare the modeled and observed regression fields, Taylor diagrams are used (Taylor 2001). These diagrams simultaneously show three characteristics describing similarity between modeled and reference fields: the root-mean-square difference normalized by the standard deviation of the reference field, the spatial correlation (r), and the ratio of the variances (η) across the spatial field.

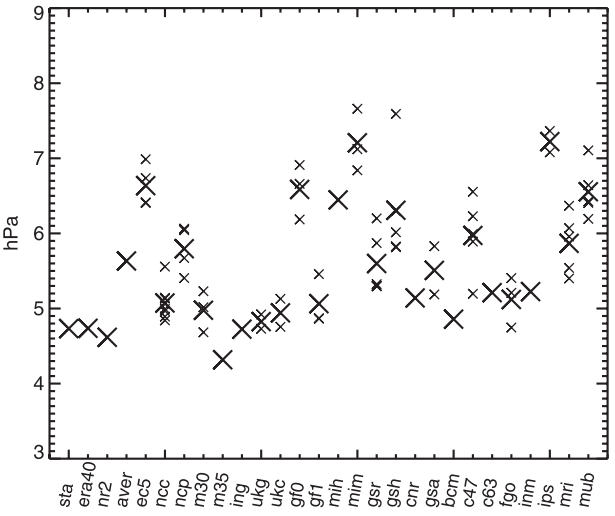

FIG. 1. Standard deviations of the SAM index in station data (sta), ERA-40, NR2, and models calculated over the period 1979–2001 for the observations and 1977–99 for the models. The standard deviation for each realization of a given model run is marked with a small bla ck cross, while the ensemble average for each model is marked with a larger black cross. Also shown is the multimodel mean standard deviation (aver).

3. Results

a. SAM pattern and variability

Figure 1 shows the standard deviations of the detrended SAM indices in all datasets used in this study. Both reanalyses SAM indices agree very well with the station-based SAM index as well as with each other. Almost all models, with the exception of the Commonwealth Scientific and Industrial Research Organisation Mark version 3.0 (CSIRO Mk3.5), show SAM index variability larger than the observations. The multimodel averaged standard deviation of the SAM index exceeds the observed standard deviation by 1 hPa (about 20%). Similar differences between simulated and observed zonal mean SLP variability are found at 40° and 65°S separately. Our results agree with Miller et al. (2006), who found that November–March EOF-based SAM index variability in the majority of the CMIP3 models exceeds that in the NCEP–National Center for Atmospheric Research (NCAR) reanalysis.

Figure 2a shows the SLP regression on the SAM index in ERA-40 and Fig. 2b shows the mean SLP

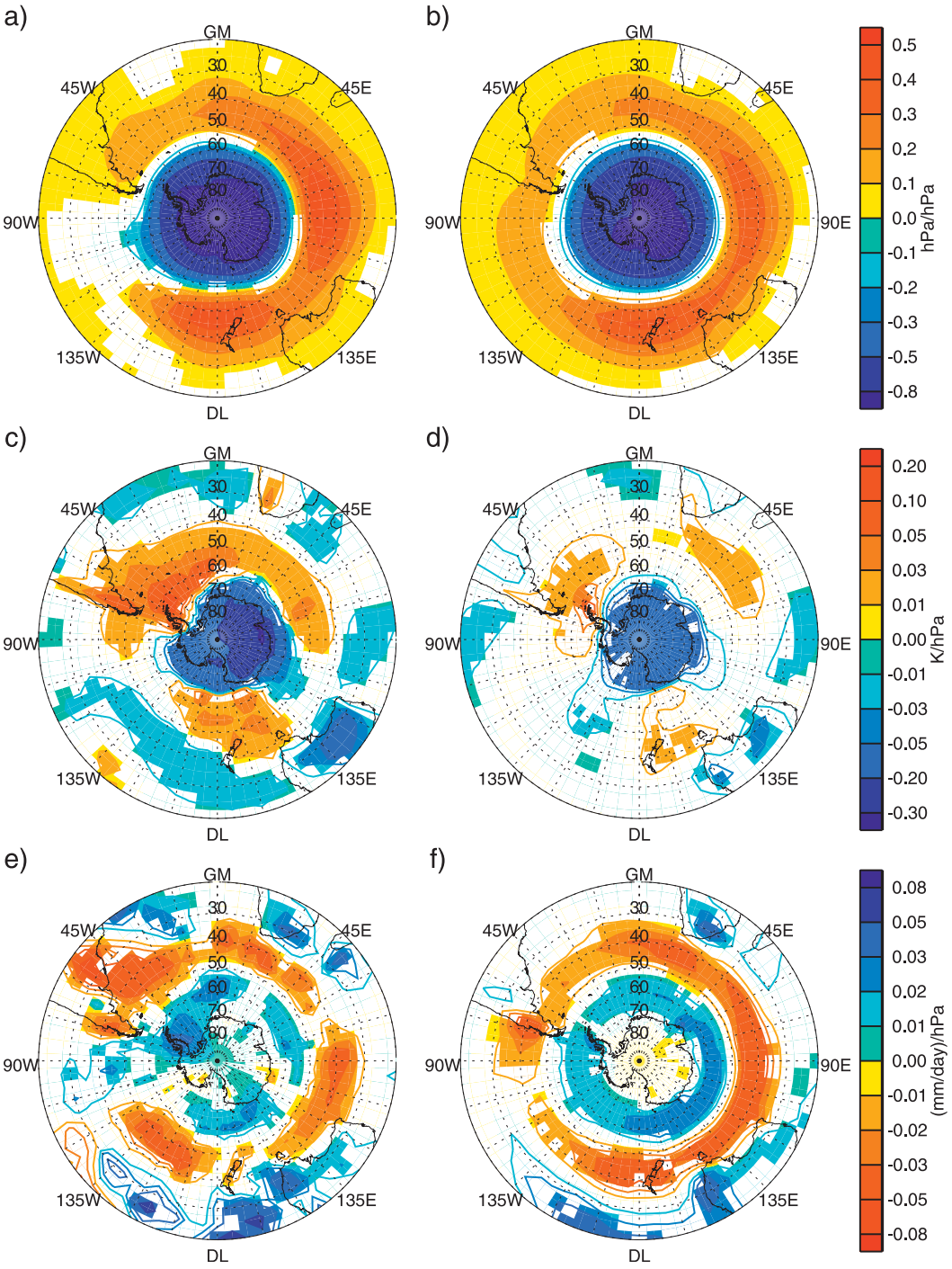

FIG. 2. Regression of (a),(b) SLP; (c),(d) surface air temperature; and (e),(f) precipitation on the SAM index in (a),(c) ERA-40; (e) GPCP; and (b),(d),(f) multimodel average. Solid contours indicate areas where (a),(c),(e) the regression is significant at the 90% significance level based on the *t* test allowing for autocorrelation; and (b),(c),(f) 95% of the models agree on the sign of the response.

regression on the SAM index in all the CMIP3 models (MULTI). The ERA-40 pattern is similar to that shown by SGE06. The observed SLP response pattern (Fig. 2a) shows zonal symmetry familiar from other studies (e.g., Thompson and Wallace 2000; Gillett et al. 2006). A major departure from zonal symmetry is an equatorward extension of the negative SLP response over the eastern Pacific between 210° and 290°E. SGE06 found

the same asymmetry in their analysis and suggested that it may be partly due to leakage between the first two modes in their EOF analysis owing to the relatively short time series used. However, the present analysis is free of possible EOF-related artifacts. Similar asymmetry was found in the Hadley Centre Sea Level Pressure (HadSLP) data over longer periods by Gillett et al. (2006), giving more credibility to the result. Note, however, that HadSLP has been made spatially complete by optimal interpolation using NCEP reanalysis EOFs and is not therefore a purely observational dataset. Lachlan-Cope et al. (2001) attributed the asymmetry to the nonaxisymmetric Antarctic orography.

Given that the El Niño–Southern Oscillation (ENSO) has an influence on SLP in the region of the zonally asymmetric response and that the SAM is weakly correlated with the ENSO in austral summer (L'Heureux and Thompson 2006), the zonal asymmetry may thought to be a manifestation of the SAM–ENSO interaction. The hypothesis was tested by removing the ENSO signal from the observed SLP field prior to regressing it on the SAM. The overall SAM response and, in particular the zonal asymmetry, do not change noticeably, suggesting that the zonal asymmetry is not attributable to the ENSO influence.

The MULTI SLP response shown in Fig. 2b is similar to that in ERA-40, suggesting that the models capture the large-scale structure of the SAM reasonably well. However, MULTI tends to be overly zonally symmetric and does not reproduce the eastern Pacific asymmetry. A similar result was found by SGE06 for the Community Climate System Model, version 2.0 (CCSM2.0) and by Raphael and Holland (2006) for several other CMIP3 models. On the other hand, the two positive centers of action around 90°E and 180° evident in the ERA-40 SLP response are captured by MULTI, albeit with somewhat reduced magnitude.

b. *Surface air temperature and total precipitation responses*

The SAT response (to the positive SAM anomaly) in ERA-40 (Fig. 2c) is dominated by cooling over Antarctica, which reaches -0.32 K hPa^{-1} in the eastern part of the continent, and warming over the Antarctic Peninsula with a maximum of 0.17 K hPa^{-1} at the northeastern tip of the peninsula. The NR2 reanalysis shows similar values. Cooling of -0.32 K hPa^{-1} corresponds to a cooling of about -0.32 K hPa$^{-1} \times 4.8$ hPa $= -1.5$ K for a one standard deviation positive anomaly of the SAM index, which is larger than values of -1 to -1.1 K reported from station observations (Thompson and Wallace 2000; Gillett et al. 2006). Because of regional effects, the cooling is not spatially uniform (van den Broeke and van Lipzig 2003) and the maximum cooling is observed inland over the East Antarctic Plateau where no station is located. The pattern of cooling obtained here is broadly consistent with that obtained from satellite data by Kwok and Comiso (2002).

A positive temperature response (Fig. 2c) covers the South Atlantic between 40° and 65°S and extends through to the southwestern Indian Ocean. A prominent warming response also occurs in the southeastern Pacific. Large areas of continental warming also exist, particularly over southern parts of South America where the warming reaches as far north as 25°S along the western coast, but also in western South Africa and over southern New Zealand and Tasmania. As discussed elsewhere (e.g., Gillett et al. 2006; SGE06), the positive anomaly in this latitude belt is linked to the positive SLP anomaly. This is associated with the descending branch of the anomalous circulation and a reduction in cloud cover and therefore is attributable to increased solar radiation. A cooling response is observed over the Australian continent where it reaches -0.07 K hPa^{-1}. As discussed by Hendon et al. (2007), the cooling is associated with weak anomalous ascent and the shading effect of clouds. Note, however, that the cooling response covers a larger area than the precipitation response (Fig. 2e), suggesting that changes in cloudiness are not the only influence on temperature. SGE06 also showed that the positive (negative) anomaly south (north) of 40°S is associated with southward (northward) advection of warm (cold) air. In general, the ERA-40 temperature response agrees well with the station analysis by Gillett et al. (2006) with only small differences. In particular, the statistically significant positive response over the Antarctic Peninsula extends farther south in ERA-40 than in the station analysis.

The multimodel mean SAT response (Fig. 2d) possesses many of the same features as in ERA-40 but is of noticeably smaller magnitude. SGE06 also noticed reduced magnitude of the SAT response in a CCSM2.0 simulation. The reduced magnitude of the simulated temperature response appears to be a common feature across the models and will be discussed in more detail later.

The precipitation response exhibits a banded pattern in both GPCP and MULTI (Figs. 2e,f); however, the response in GPCP appears weaker south of 35°S. The band of positive response at ~55°–70°S and the band of negative response between 35° and 50°S coincide with the negative and positive pressure anomalies and corresponding regions of anomalous ascent and descent,

respectively. The band of negative response covers, in particular, New Zealand, Tasmania, the extreme southeast and extreme southwest of Australia, the extreme southwest of South Africa, and the southern part of South America and was discussed in regional studies (Reason and Rouault 2005; Meneghini et al. 2007; Cai and Cowan 2006). Anomalies north of 35°S are less zonally symmetric. In both GPCP and MULTI, southern Australia and eastern South Africa show increased precipitation in agreement with the station analysis by Gillett et al. (2006). Hendon et al. (2007) attributed the moistening response observed on the east coast of Australia to advection of moist air from the ocean by anomalous easterly winds. However, this argument may not apply inland away from the coast. Cai and Cowan (2006), Hendon et al. (2007), and Shi et al. (2008) demonstrated that the drying response over the extreme south of Australia maximizes in winter and the moistening response over the east coast maximizes in summer in association with seasonal meridional migration of the SAM pattern.

The GPCP and MULTI precipitation responses disagree over the eastern Antarctic Peninsula and the Weddell Sea where the GPCP response shows a local maximum, which is absent in MULTI. The maximum is absent in ERA-40 too (not shown). The high topography of the Antarctic Peninsula creates a precipitation shadow region on the eastern side of the peninsula (Turner et al. 1995), therefore the maximum appears unexpected, at least in the northern part of the region where a more positive SAM index is associated with the more frequent passage of air from west to east of the peninsula (Marshall et al. 2006). MULTI does not reproduce the equatorward extension of the moistening response over the eastern Pacific Ocean evident in GPCP. This is most probably related to the models' failure to reproduce the negative pressure anomaly in this region. Another area of disagreement between MULTI and GPCP is along the east coast of South America between 20° and 40°S. Here, GPCP shows a negative precipitation response, which is absent in MULTI. Gillett et al. (2006) show one station in this region with significant drying response. Silvestri and Vera (2003) showed that the response in this region is largest in late spring. They suggested that the response is linked to a SAM-related positive pressure anomaly that blocks the moisture transport by cyclones. If so, this mechanism is apparently missing in the models.

Figure 3a is a Taylor diagram of the SAT response to the SAM index for individual models as well as for MULTI. The similarity of models to ERA-40 can be assessed in terms of the normalized rms difference, the spatial correlation r, and the ratio of the variances η. The radial distance from the origin represents the ratio of standard deviations η while the cosine of the angle from the horizontal axis is equal to the spatial correlation coefficient r. The distance from the point (1,1) located on the horizontal axis represents the ratio of the centered pattern rms error to the standard deviation of the ERA-40 response.

Table 2 shows the values of r and η for MULTI, reanalyses, and observed datasets as well as the range and the mean values across individual models. The correlation between the mean simulated and observed temperature response to the SAM is high. However, η is only about 0.5, reflecting the fact noticed earlier that the models underestimate the magnitude of the response. The results suggest that it is the magnitude of the SAM response that is the problem for the models and not the spatial pattern, which is captured by all the models reasonably well. Reassuringly, the NR2 reanalysis shows the best agreement with ERA-40 in terms of both r and η, suggesting that the choice of the reference dataset has not strongly influenced the results of this evaluation.

Figure 3b is a Taylor diagram of the precipitation response to the SAM. MULTI shows better agreement with GPCP in terms of rms difference and in terms of spatial correlation than any individual model (Table 2). The agreement between GPCP and CMAP is good; however, the differences between GPCP and the reanalyses are larger than that between GPCP and MULTI. The magnitude of the response is larger in both ERA-40 and NR2 than in GPCP. Both reanalyses are in better agreement with the models than are GPCP and CMAP, which may be because the reanalysis models are not constrained directly by precipitation measurements and respond to the SAM similarly to the CMIP3 models. The mean rms difference between the models and ERA-40 is only 0.78, which is smaller than the mean rms difference between the models and GPCP (1.06). Considerable differences between the precipitation responses in observed datasets (GPCP and CMAP) and the reanalyses are at odds with the conclusion by SGE06 that the responses are insensitive to the dataset used.

The small values of η for the SAT regression indicate that the models underestimate the SAT responses to SAM. However, this provides no information about over which regions the responses are underestimated. Figures 4a–d show the averaged area-weighted SAT response to the SAM in the models and in ERA-40 in four regions (continental Antarctica, the Antarctic Peninsula, Australia, and South America south of 30°S) where the SAT response is largest. The other land regions impacted by the SAM (South Africa, southern

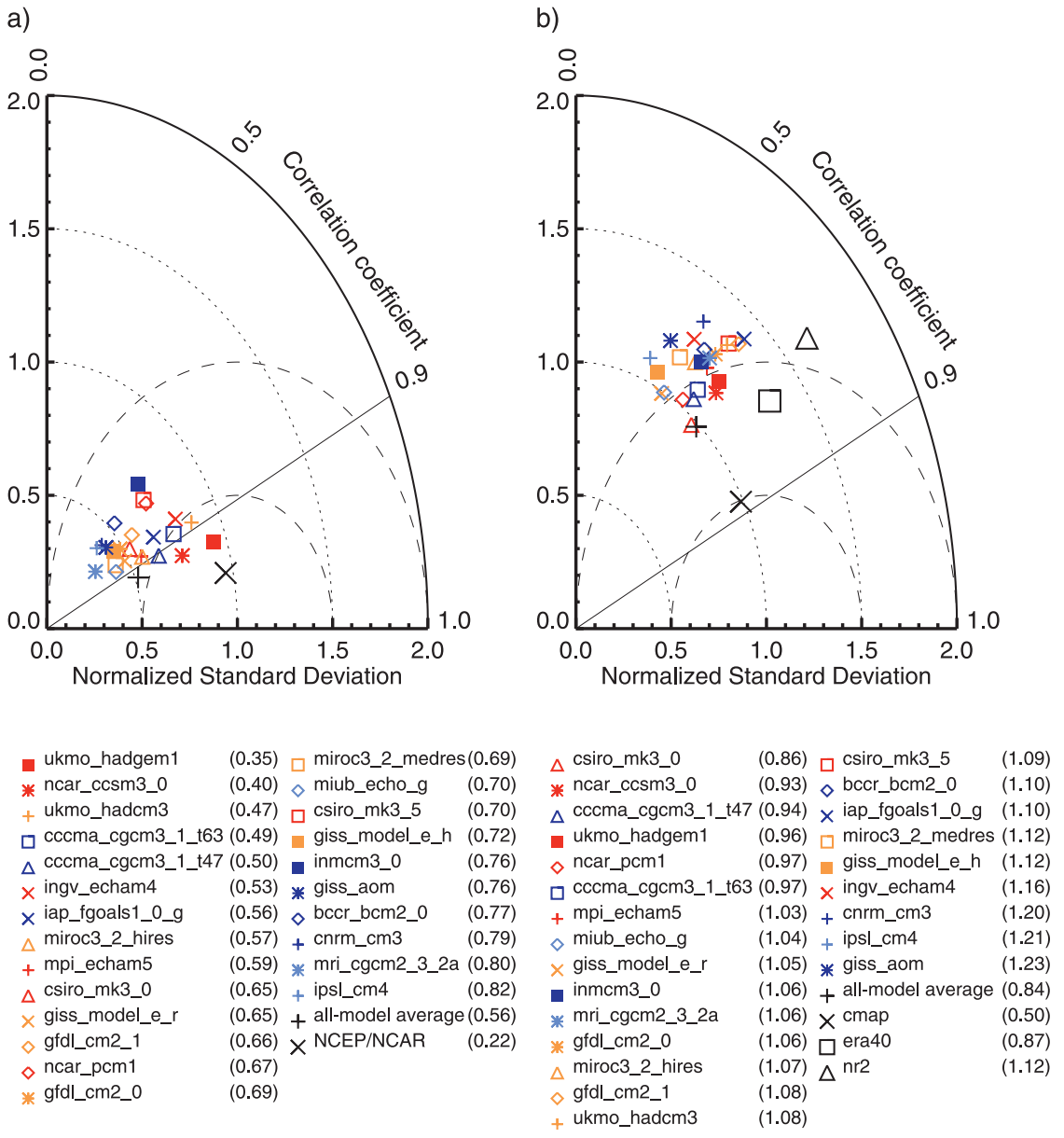

FIG. 3. Taylor diagram showing the resemblance between (a) surface air temperature and (b) precipitation regressions on the SAM index from the models, ERA-40, and GPCP. The numbers in parentheses next to model names represent normalized rms differences.

New Zealand, and Tasmania) are of substantially smaller size and will not be considered here.

Across the Antarctic continent, excluding the peninsula (Fig. 4a), ERA-40 shows an averaged cooling of −0.19 K hPa^{-1}, while the multimodel average shows only about half as much cooling. Individual models show a large spread of values, with the weakest response being only −0.05 K hPa^{-1}. The two Met Office (UKMO) models show the best agreement with the observations (−0.18 K hPa^{-1}). Overall, the models underestimate the temperature response to SAM over the Antarctic continent and also in the free troposphere, as shown in Fig. 4e. Monaghan et al. (2008) analyzed five CMIP3 models and found that the correlation coefficients between detrended continent-averaged SAT and detrended SAM index in the models are comparable to those in the observations. However, they did not compare the regression coefficients to test the similarity of the absolute values of the response.

The warming response over the Antarctic Peninsula (Fig. 4b) is also typically underestimated, although the ERA-40 value is within the 2.5%–97.5% interval

TABLE 2. The spatial correlation r and the ratio of the variances η for the responses to the SAM. The reference dataset is shown as a subscript for PRE and SST.

Variable		Individual models			MULTI	ERA-40	NR2	GPCP	CMAP	HadISST	NOAA OI
		Mean	Min	Max							
SAT	r	0.81	0.67	0.94	0.93	—	0.98	—	—	—	—
	η	0.59	0.33	0.93	0.49	—	0.96	—	—	—	—
PRE_{GPCP}	r	0.54	0.36	0.64	0.64	0.77	0.74	—	0.88	—	—
	η	1.18	0.98	1.40	0.99	1.33	1.63	—	0.99	—	—
PRE_{ERA40}	r	0.68	0.54	0.76	0.80	—	0.86	0.77	0.74	—	—
	η	0.89	0.73	1.05	0.74	—	1.23	0.75	0.78	—	—
$SST_{HadISST}$	r	0.51	0.24	0.67	0.63	—	—	—	—	—	0.91
	η	1.56	0.87	2.19	1.38	—	—	—	—	—	1.36
$SST_{NOAA\ OI}$	r	0.51	0.35	0.67	0.61	—	—	—	—	0.91	—
	η	1.16	0.64	1.64	1.02	—	—	—	—	0.94	—
SIC	r	0.21	−0.26	0.53	0.57	—	—	—	—	—	—
	η	0.50	0.27	0.82	0.20	—	—	—	—	—	—

of the model values. The majority of the models show a positive response, with the exception of the GISS Atmosphere–Ocean Model (AOM) and L'Institut Pierre-Simon Laplace Coupled Model version 4 (IPSL CM4). In these two models the positive response is weak and shifted north, resulting in the net negative response over the peninsula. MULTI shows a warming of 0.04 K hPa^{-1}, which is less than half of the ERA-40 value (0.10 K hPa^{-1}). Only the Bjerknes Centre for Climate Research Bergen Climate Model version 2.0 (BCCR BCM2.0) shows slightly larger warming than ERA-40 (0.11 K hPa^{-1}).

The response over southern South America (Fig. 4c) is much smaller in magnitude than that over Antarctic, and several models do not capture the positive response over this region. These models show a strong negative response over eastern South America between 30° and 40°S, which dominates over the positive response farther south when averaged over the region.

Among the four regions only in Australia is the magnitude of observed response within the 2.5%–97.5% range of model responses (Fig. 4d). The magnitude of the MULTI response is -0.02 K hPa^{-1}, which is similar to -0.03 K hPa^{-1} in ERA-40. Several models show a stronger response than that in ERA-40. All but two models [Institute of Numerical Mathematics Coupled Model, version 3.0 (INM-CM3.0), IPSL CM4] show a cooling response over the region as observed.

Although the results are based on detrended data, one may speculate that the differences in forcing between the models influence their temperature responses to the SAM. We tested this hypothesis by analyzing Hadley Centre Global Environmental Model version 1 (HadGEM1) runs with anthropogenic and natural, greenhouse-gas-only, and anthropogenic-only forcing and found no significant difference in the temperature response.

c. *Sea surface temperature and sea ice concentration responses*

Figure 5 shows the SST response to the SAM in HadISST and in MULTI. Due to the thermal inertia of the ocean the maximum response of SST and SIC to the SAM is delayed by approximately one month (SGE06). Thus, the one-month lagged SST and SIC time series are used for the regression on SAM. The spatial pattern of HadISST SST response (Fig. 5a) is very similar to that of NOAA OI SST shown by SGE06. There are negative centers of action in the central parts of South Pacific (south of 30°S) and Indian (south of 50°S) Oceans. The band of positive response between 30° and 50°S extends across the South Atlantic and the western Indian Ocean to 90°E. Another area of positive response is located southeast of Australia surrounding New Zealand and Tasmania. The observed zonal asymmetry of the response contrasts with the strongly symmetric response evident in MULTI (Fig. 5b). Screen et al. (2009) showed that the observed negative SST response over the Pacific is associated with negative anomalies in the observed atmosphere-to-ocean heat fluxes, and the observed positive SST response east of Drake Passage is associated with positive anomalies in atmosphere-to-ocean heat fluxes. They suggest that the observed atmosphere-to-ocean heat flux anomalies in these regions are associated with observed zonal asymmetry in the SLP response, which is not simulated by the models. SGE06 arrived at a similar conclusion. Away from these regions the simulated SST response is of noticeably larger magnitude than the observed one.

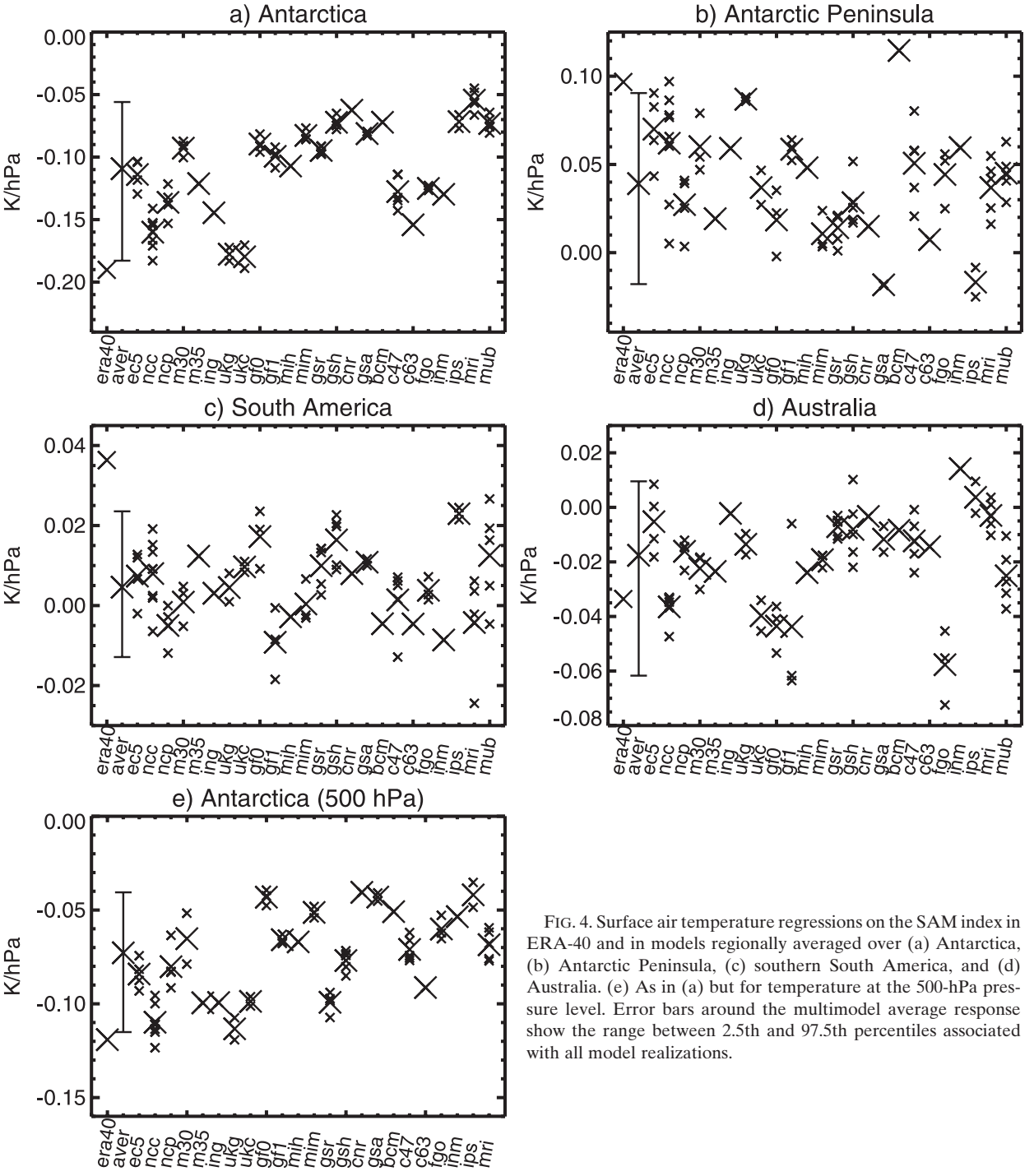

FIG. 4. Surface air temperature regressions on the SAM index in ERA-40 and in models regionally averaged over (a) Antarctica, (b) Antarctic Peninsula, (c) southern South America, and (d) Australia. (e) As in (a) but for temperature at the 500-hPa pressure level. Error bars around the multimodel average response show the range between 2.5th and 97.5th percentiles associated with all model realizations.

A Taylor diagram for the SST response is shown in Fig. 5c. The majority of the models have η larger than 1, which reflects a consistent tendency to overestimate the magnitude of the SST response by the models (see also Fig. 6 and Table 2). NOAA OI SST shows noticeably better agreement with HadISST than any of the models in terms of spatial pattern correlation. However, the difference between the two datasets is quite large (rms = 0.63). The magnitude of the SST response in NOAA OI SST is larger than that in HadISST and is in better agreement with the models (Fig. 5d and Table 2). The stronger magnitude of the NOAA OI SST response is

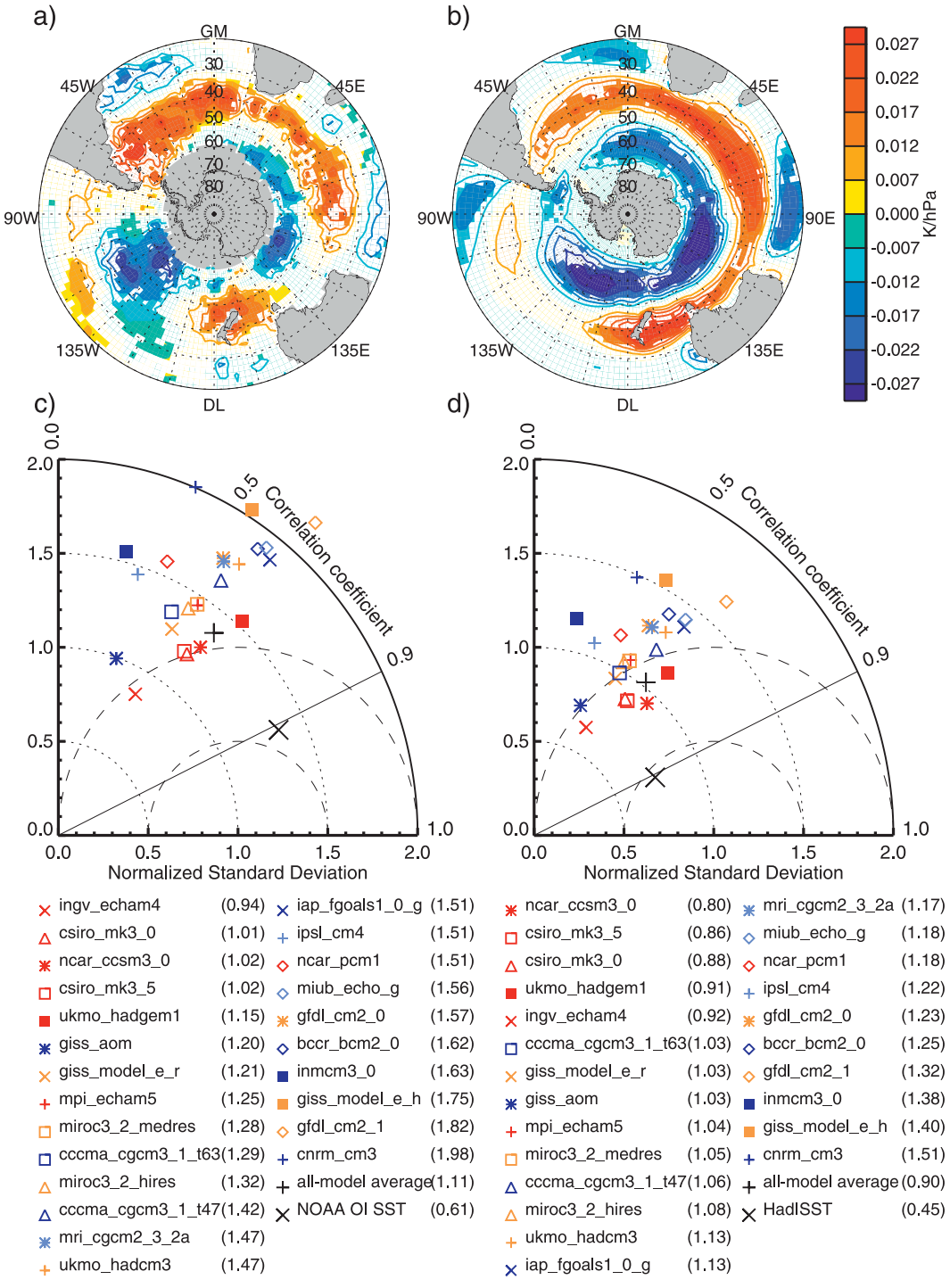

FIG. 5. Regression of sea surface temperature on the SAM index for (a) HadISST and (b) the multimodel average. Solid contours indicate areas where (a) the regression is significant at the 90% significance level based on a t test allowing for autocorrelation and (b) 95% of the models agree on the sign of the response; Taylor diagrams showing the resemblance between sea surface temperature regressions on the SAM index from the models and (c) HadISST and (d) NOAA OI SST. Numbers in parentheses next to model names represent normalized rms differences.

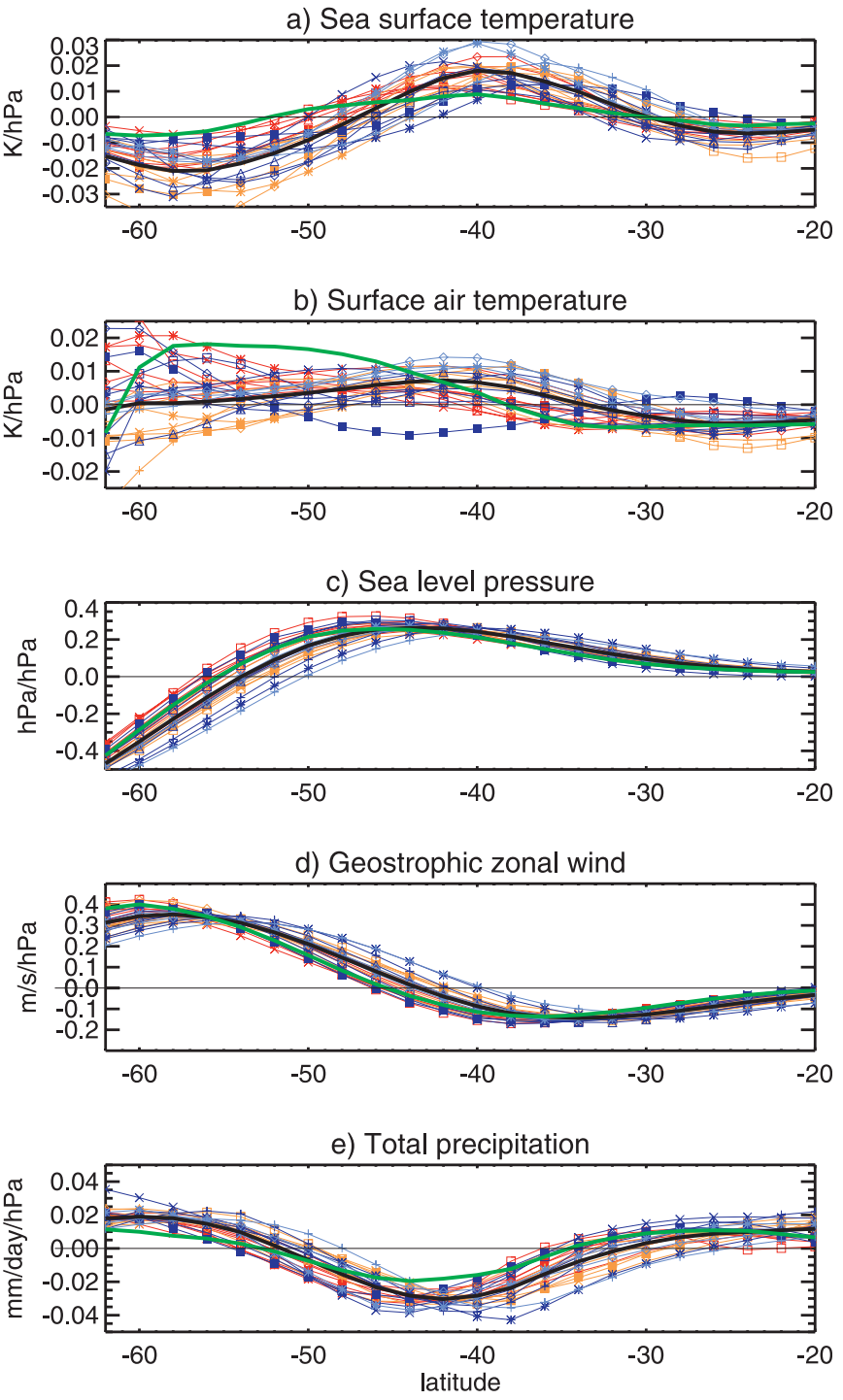

FIG. 6. Ocean-only zonally averaged (a) sea surface temperature, (b) surface air temperature, (c) sea level pressure, (d) geostrophic zonal wind, and (e) total precipitation regressions on the SAM index in the models, HadISST, ERA-40, and GPCP. The thick green line indicates observations or reanalysis, the thick black line indicates the multimodel average, and individual models are indicated by the same symbols as in Fig. 3.

associated with larger monthly SST variability in this dataset compared to HadISST. The mean standard deviation averaged south of 20°S is about 0.38 K in HadISST and 0.51 K in NOAA OI SST. The latter value is comparable to that in the multimodel average (0.49 K). The reduced standard deviation in HadISST has previously been reported by Rayner et al. (2003). Both HadISST and NOAA OI SST are based on essentially the same input sources but use different techniques to interpolate data to regions where no observations are available. HadISST uses the reduced space optimum interpolation technique, which retains only information contained in the lowest-order empirical orthogonal functions. This reduces noise associated with observational errors but may also reduce the variance (see Rayner et al. 2003 for more detailed discussion).

Figure 6 shows zonal mean SST, SAT, SLP, PRE, and zonal geostrophic wind responses to the SAM index in models and in observations. All of the quantities are averaged over ocean only. Clearly, the SST and SAT over ocean (SATO) responses show the worst agreement with the observations. The poor simulation of the SATO response reveals that the relatively good simulation of the overall SAT response is primarily because the models realistically capture the dominant features over the continents. Simulated patterns of zonal mean SLP and geostrophic zonal wind responses are in a better agreement with the observations but shifted north of the observed patterns by several degrees. The magnitudes of the simulated PRE response are larger than that in GPCP.

All models overestimate the surface cooling in the Southern Ocean at 50°–60°S as well as underestimating the warming of the overlying SATO. Some of the models simulate negative zonal mean SATO response contrary to the observations. There is a tendency for models with a more positive SATO response to show a less negative SST response at 50°–60°S and to be in better agreement with the observations. A correlation across the models between the simulated SATO and SST responses at 48°–62°S is statistically significant at the 99% level ($r \sim 0.7$).The coupling between SST and SATO responses is also observed at 35°–45°S where the models overestimate the SST warming. In principle SST anomalies could drive SATO anomalies through modified atmosphere–ocean heat fluxes. SGE06 showed that this process becomes important on time scales longer than the initial SAM response. However, Screen et al. (2009), studying the initial SST response to the SAM, show that in most of the Southern Ocean the ocean–atmosphere heat fluxes are associated with SATO anomalies driving SST anomalies rather than the other way round.

The errors in simulated SST response may also be related to possible errors in simulating meridional heat advection by SAM-induced Ekman flow, which is controlled by anomalous zonal surface wind. Indeed, there is a correlation across the models between the simulated eastward geostrophic zonal wind and SST responses at 48°–62°S that is statistically significant at the 99% level ($r \sim -0.6$). This implies that the models indicating a colder SST response have stronger anomalous equatorward Ekman transport of cold water. Among the models, only the Istituto Nazionale di Geofisica e Vulcanologia SINTEX-G (INGV-SXG) has the average geostrophic zonal wind response weaker than that in ERA-40. Note that the magnitude of the correlation coefficient is somewhat sensitive to the latitude band chosen, and there is no such correlation between SST and wind responses at 35°–45°S where the models simulate a too warm SST response. Screen et al. (2009) analyzed the SAM responses in four CMIP3 models and found that in their subset all of the models simulated a too-strong anomalous Ekman flow related to a too-strong zonal wind response. They concluded that the errors in the simulated Ekman heat flux are larger than the other mixed layer heat budget terms over most latitudes within 40°–65°S. North of 40°S, errors in the atmosphere-to-ocean heat fluxes become increasingly important.

The observed pattern of SIC response (Fig. 7a) consists of a negative response in the eastern part of the Bellingshausen Sea and northeast of the Antarctic Peninsula, a negative response between 135° and 165°E, and three centers of positive response in the 0°–50°E, 90°–135°E, and 165°–260E° sectors. Note that the SIC response resembles a southward extension of the SST response, with areas of positive SST response corresponding to areas of negative SIC response and vice versa. Sea ice changes are driven by atmospheric and oceanic heat flux convergence as well as by wind and oceanic advection. All of these factors are influenced by SAM variability. In a model study Hall and Visbeck (2002) found primarily a positive SIC response to the SAM that they attributed to equatorward advection of ice by SAM-induced Ekman drift. However, this picture is not consistent with the observations. SGE06 showed that the SIC response in some regions can be attributed to advection by anomalous westerlies and anomalous eastward oceanic currents. In this case, the sign of response depends on orientation of the ice edge. In Drake Passage and in the western South Atlantic the orientation of the climatological ice edge is northeastward. Therefore the westward advection in that region reduces ice extent, thus resulting in a strong negative response. SGE06 suggested that the positive SAT response to

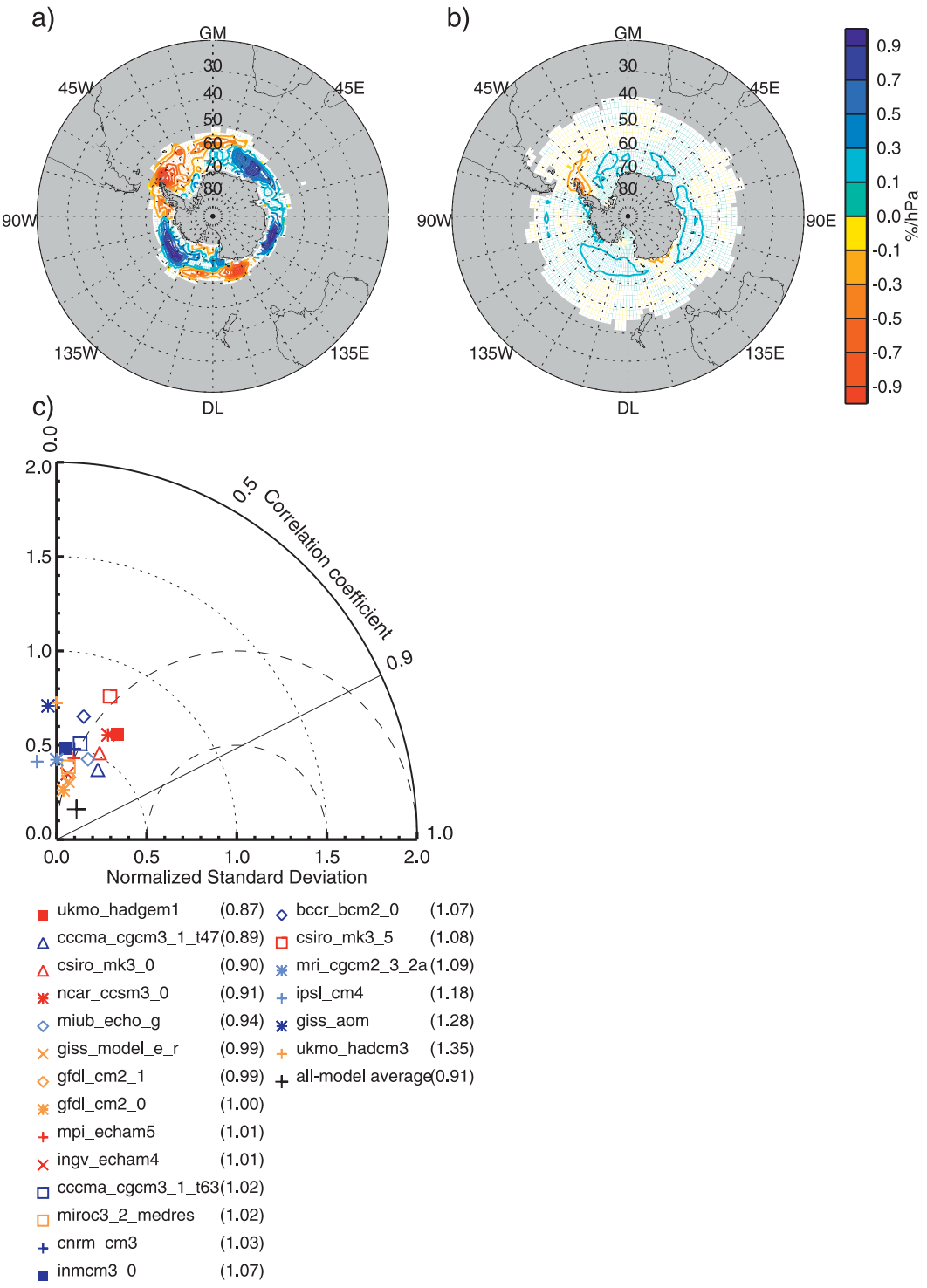

FIG. 7. As in Figs. 5a–c, but for sea ice concentration. The multimodel average at each point in Fig. 7b is calculated only over simulations showing ice variability at that point. Thus, the number of ensemble members differs from point to point. The area where no simulation exhibits ice variability is shaded.

SAM in that region also contributes to the negative SIC response. In a similar manner, the positive responses in Fig. 7a coincide with the regions where the climatological ice edge is oriented southeastward; therefore, the westward advection would extend ice fields there. These regions also coincide with regions of negative SAT response to the SAM (Fig. 2c). Similarly, the negative response in the Australian sector is overlaid by a positive SAT response.

The multimodel mean simulated pattern of SIC response (Fig. 7b) reveals the major features of the observed response, although the magnitude of the response is considerably reduced. The negative response around the Antarctic Peninsula extends east only to 30°W, while the observed response is stronger and extends farther east to 15°E. In a similar manner, the simulated increase in sea ice in the northern part of the Ross Sea is weaker and covers less area than that observed. The negative response centered to the south of Tasmania, which is pronounced in HadISST, is confined to the coast and weaker in MULTI. Only in the small area northeast of the Antarctic Peninsula do 95% of the models agree on the sign of the response. A weaker simulated response in winter and summer seasons separately was earlier noticed by SGE06 in CCSM2.0.

The Taylor diagram for the SIC response (Fig. 7c) shows that the response is simulated poorly by individual models. In terms of the spatial pattern, MULTI shows better agreement with HadISST than any individual model (Table 2). However, the value of η is only 0.20, indicating that the magnitude of the response is substantially underestimated by MULTI. Individual models perform poorly in terms of both spatial pattern and the magnitude of the response. The magnitude of the response is underestimated by all the models.

Among the models, only the third climate configuration of the Met Office Unified Model (UKMO HadCM3) simulates the zonally symmetric response seen by Hall and Visbeck (2002). The ice advection in this model is driven purely by the oceanic current, suggesting that the response may be dominated by SAM-induced equatorward Ekman drift.

Note that the annual mean SIC climatology is simulated reasonably well by the majority of the models studied here (not shown), although there is a bias toward low SIC compared to HadISST. Connolley and Bracegirdle (2007) in their analysis of 15 CMIP3 models showed that the best models in simulating SIC climatology are the Meteorological Research Institute Coupled General Circulation Model version 2.3.2 (MRI CGCM2.3.2) and CSIRO Mk3.0. However, we find that MRI CGCM2.3.2 is not among the best in simulating the SAM response and that, in general, there is little correlation between abilities of individual models to simulate the climatology and the SAM response. Similarly to UKMO HadCM3, MRI CGCM2.3.2 does not include wind advection of ice fields, but the response in this model is not zonally symmetric. Another model, INM-CM3.0, does not include ice dynamics at all. Not surprisingly, the SIC response in this model bears little resemblance to the observed response.

Since mean ice conditions are very different between summer and winter seasons, the responses to the SAM could also be very different. Similar analysis performed for the two seasons separately showed that the model skills in simulating the sea ice response are poor in both seasons, similar to the annual case (not shown). The annual SIC response is dominated by the winter response in both observations and models, with a smaller contribution from the summer response.

4. Discussion and conclusions

SGE06 analyzed climate impacts of the SAM in CCSM2.0 and identified several model deficiencies, such as the underestimation of SAT and sea ice responses to the SAM and the too strong and too zonal response in SST. Here we extend these results to provide a more quantitative evaluation of the responses across the full set of CMIP3 models to show that the above deficiencies are common across all analyzed models.

In general, the CMIP3 models satisfactorily reproduce the large-scale spatial pattern of SAT response to the SAM; however, the magnitude of response is underestimated by the majority of models. In absolute terms, the greatest underestimation of the response occurs over the Antarctic continent where the observed SAT response is strongest. The response is largely determined by the wind field response (van den Broeke and van Lipzig 2003). Therefore, model deficiencies in reproducing the SAT response may be associated, at least partly, with discrepancies in the wind response and heat advection. Physical parameterizations in the models may be another source of the discrepancies. The models also underestimate the cooling in the free troposphere, suggesting that parameterization of the boundary layer is unlikely to be an important source of the discrepancies.

Underestimation of the SAT response by the models implies that the SAT changes associated with future SAM changes will also be underestimated, assuming that the SAM–temperature relationship on a long-term scale is similar to that on monthly scale, and that the

overall temperature response is a sum of responses to different forcing agents (Meehl et al. 2004).

Analysis of the precipitation response reveals important regional discrepancies between observed and simulated patterns, such as a missing moistening response over the eastern Antarctic Peninsula in the simulations, but also large discrepancies between the observed datasets (GPCP and CMAP) and the reanalyses (ERA-40, NR2). Similarly to the models, the reanalyses do not reproduce a maximum in the precipitation response over the eastern Antarctic Peninsula. Also, the magnitude of the response in the reanalyses appears larger than in the observed datasets and is more comparable to the models. Precipitation in the reanalyses is strongly controlled by the physics of the underlying general circulation model, which makes them less reliable references than the observed datasets. However, the observed datasets also suffer from substantial uncertainties (Adler et al. 2003). Differences between the precipitation responses across the reference datasets add uncertainty to the evaluation of the simulated precipitation response.

The simulated SST response to the SAM is too strong and too zonal. Model biases in the SST response are coupled with biases in the overlying SAT response. Models that simulate stronger zonal wind response also simulate stronger SST response, implying that errors in simulating anomalous meridional heat advection by Ekman flow likely contribute to the errors in the simulated SST response. This is confirmed by Screen et al. (2009), who performed a detailed study of the terms of the ocean mixed layer heat budget. While the simulations only possess limited skill in representing the short-term SST response to the SAM, the long-term response, which is influenced by mesoscale eddies, may be even more questionable (i.e., Screen et al. 2009).

As for precipitation, our evaluation of the SST response to the SAM suffers from uncertainties in the observational data. While the responses in HadISST and NOAA OI SST data show similar spatial patterns, the magnitude of the NOAA OI SST response is about 30% larger, corresponding to generally larger monthly variability in this dataset that is better matched with the models. Owing to these uncertainties in the observations, it is difficult to assess the degree to which the magnitudes of observed and simulated SST responses differ.

Finally, the largest problems are identified in simulating the sea ice response to the SAM. Although the response in some models is broadly consistent with the observations, other models are not able to reproduce the observed spatial pattern of response at all. All of the models strongly underestimate the magnitude of SIC response. In some models, the poor performance can be related to a simplified representation of sea ice. However, the majority of the models include a quite sophisticated sea ice component and the reason for their shortcomings in simulating the sea ice response to the SAM is less clear. Like the SAT, the sea ice response is influenced by anomalous wind fields. Significant biases in the SLP response and associated geostrophic winds exist in the models. Some of the errors in the simulated wind response will translate into sea ice response biases. Taking into account projected SAM trends, problems detected in the simulated SIC response will likely influence projected SIC changes, and therefore they need to be addressed in model development.

This comprehensive analysis uses quantitative metrics to provide estimates of model biases related to the climate impacts of the SAM on monthly time scales. The results may be useful in interpreting simulations of future Southern Hemisphere climate change.

Acknowledgments. This work is supported by NERC Project NE/E006787/1. We acknowledge the modeling groups, the Program for Climate Model Diagnosis and Intercomparison (PCMDI) and the WCRP's Working Group on Coupled Modelling (WGCM) for their roles in making available the WCRP CMIP3 multimodel dataset. Support of this dataset is provided by the Office of Science, U.S. Department of Energy. ECMWF is acknowledged for providing ERA-40 data. The HadISST dataset was assembled by the UKMO Hadley Centre and obtained through the BADC, available online at http://www.badc.nerc.ac.uk/. NCEP DOE AMIP II Reanalysis, NOAA OI SST V2, GPCP, and CMAP data are provided by the NOAA/OAR/ESRL PSD, Boulder, Colorado, from their Web site at http://www.cdc.noaa.gov/. We thank Adam Scaife for providing HadGEM1 data and three anonymous reviewers for their comments. The manuscript has benefited from useful comments from David Thompson. NPG acknowledges support from the Leverhulme Trust.

REFERENCES

Adler, R. F., and Coauthors, 2003: The version 2 Global Precipitation Climatology project (GPCP) monthly precipitation analysis (1979–present). *J. Hydrometeor.,* **4,** 1147–1167.

Arblaster, J. M., and G. A. Meehl, 2006: Contributions of external forcings to southern annular mode trends. *J. Climate,* **19,** 2896–2905.

Boer, G. J., S. Fourest, and B. Yu, 2001: The signature of the annular modes in the moisture budget. *J. Climate,* **14,** 3655–3665.

Brahmananda Rao, V., A. M. C. do Carmo, and S. Franchito, 2003: Interannual variations of storm tracks in the Southern Hemi-

sphere and their connections with the Antarctic Oscillation. *Int. J. Climatol.,* **23,** 1537–1545.

Cai, W., and I. G. Watterson, 2002: Modes of interannual variability of the Southern Hemisphere circulation simulated by the CSIRO climate model. *J. Climate,* **15,** 1159–1174.

——, and T. Cowan, 2006: SAM and regional rainfall in IPCC AR4 models: Can anthropogenic forcing account for southwest Western Australian winter rainfall reduction? *Geophys. Res. Lett.,* **33,** L24708, doi:10.1029/2006GL028037.

——, and ——, 2007: Trends in Southern Hemisphere circulation in IPCC AR4 models over 1950–99: Ozone depletion versus greenhouse forcing. *J. Climate,* **20,** 681–693.

——, G. Shi, and Y. Li, 2005: Multidecadal fluctuations of winter rainfall over southwest Western Australia simulated in the CSIRO Mark 3 coupled model. *Geophys. Res. Lett.,* **32,** L12701, doi:10.1029/2005GL022712.

Chapman, W. L., and J. E. Walsh, 2007: A synthesis of Antarctic temperatures. *J. Climate,* **20,** 4096–4117.

Connolley, W. M., and T. J. Bracegirdle, 2007: An Antarctic assessment of IPCC AR4 coupled models. *Geophys. Res. Lett.,* **34,** L22505, doi:10.1029/2007GL031648.

Gillett, N. P., and D. W. J. Thompson, 2003: Simulation of recent Southern Hemisphere climate change. *Science,* **302,** 273–275.

——, T. D. Kell, and P. D. Jones, 2006: Regional climate impacts of the Southern Annular Mode. *Geophys. Res. Lett.,* **33,** L23704, doi:10.1029/2006GL027721.

Gong, D., and S. Wang, 1999: Definition of Antarctic Oscillation index. *Geophys. Res. Lett.,* **26,** 459–462.

Hall, A., and M. Visbeck, 2002: Synchronous variability in the Southern Hemisphere atmosphere, sea ice, and ocean resulting from the annular mode. *J. Climate,* **15,** 3043–3057.

Hendon, H. H., D. W. J. Thompson, and M. C. Wheeler, 2007: Australian rainfall and surface temperature variations associated with the Southern Hemisphere annular mode. *J. Climate,* **20,** 2452–2467.

Holland, M. M., and M. N. Raphael, 2006: Twentieth century simulation of the Southern Hemisphere climate in coupled models. Part II: Sea ice conditions and variability. *Climate Dyn.,* **26,** 229–245.

Kanamitsu, M., W. Ebisuzaki, J. Woollen, S.-K. Yang, J. J. Hnilo, M. Fiorino, and G. L. Potter, 2002: NCEP–DOE AMIP-II Reanalysis (R-2). *Bull. Amer. Meteor. Soc.,* **83,** 1631–1643.

Kwok, R., and J. Comiso, 2002: Spatial patterns of variability in Antarctic surface temperature: Connections to the Southern Hemisphere annular mode and the Southern Oscillation. *Geophys. Res. Lett.,* **29,** 1705, doi:10.1029/2002GL015415.

Lachlan-Cope, T. A., W. M. Connolley, and J. Turner, 2001: The role of the non-axisymmetric Antarctic orography in forcing the observed pattern of variability of the Antarctic climate. *Geophys. Res. Lett.,* **28,** 4111–4114.

Lefebvre, W., H. Goosse, R. Timmermann, and T. Fichefet, 2004: Influence of the Southern Annular Mode on the sea ice–ocean system. *J. Geophys. Res.,* **109,** C09005, doi:10.1029/2004JC002403.

L'Heureux, M. L., and D. W. J. Thompson, 2006: Observed relationships between the El Niño–Southern Oscillation and the extratropical zonal-mean circulation. *J. Climate,* **19,** 276–287.

Li, Y., W. Cai, and E. P. Campbell, 2005: Statistical modeling of extreme rainfall in southwest Western Australia. *J. Climate,* **18,** 852–863.

Liu, J., J. A. Curry, and D. G. Martinson, 2004: Interpretation of recent Antarctic sea ice variability. *Geophys. Res. Lett.,* **31,** L02205, doi:10.1029/2003GL018732.

Marshall, G. J., 2003: Trends in the southern annular mode from observations and reanalyses. *J. Climate,* **16,** 4134–4143.

——, 2007: Half-century seasonal relationships between the Southern Annular Mode and Antarctic temperatures. *Int. J. Climatol.,* **27,** 373–383.

——, P. A. Scott, J. Turner, W. M. Connolley, J. C. King, and T. A. Lachlan-Cope, 2004: Causes of exceptional atmospheric circulation changes in the Southern Hemisphere. *Geophys. Res. Lett.,* **31,** L14205, doi:10.1029/2004GL019952.

——, A. Orr, N. P. M. van Lipzig, and J. C. King, 2006: The impact of a changing Southern Hemisphere annular mode on Antarctic Peninsula summer temperatures. *J. Climate,* **19,** 5388–5404.

Meehl, G. A., W. M. Washington, C. M. Ammann, J. M. Arblaster, T. M. L. Wigley, and C. Tebaldi, 2004: Combinations of natural and anthropogenic forcings in twentieth-century climate. *J. Climate,* **17,** 3721–3727.

Meneghini, B., I. Simmonds, and I. N. Smith, 2007: Association between Australian rainfall and the southern annular mode. *Int. J. Climatol.,* **27,** 109–121.

Miller, R. L., G. A. Schmidt, and D. T. Shindell, 2006: Forced annular variations in the 20th century Intergovernmental Panel on Climate Change fourth assessment report models. *J. Geophys. Res.,* **111,** D18101, doi:10.1029/2005JD006323.

Mo, K. C., 2000: Relationships between low-frequency variability in the Southern Hemisphere and sea surface temperature anomalies. *J. Climate,* **13,** 3599–3610.

Monaghan, A. J., D. H. Bromwich, and D. P. Schneider, 2008: Twentieth century Antarctic air temperature and snowfall simulations by IPCC climate models. *Geophys. Res. Lett.,* **35,** L07502, doi:10.1029/2007GL032630.

Parkinson, C. L., K. Y. Vinnikov, and D. J. Cavalieri, 2006: Evaluation of the simulation of the annual cycle of Arctic and Antarctic sea ice coverages by 11 major global climate models. *J. Geophys. Res.,* **111,** C07012, doi:10.1029/2005JC003408.

Perlwitz, J., S. Pawson, R. L. Fogt, J. E. Nielsen, and W. D. Neff, 2008: Impact of stratospheric ozone hole recovery on Antarctic climate. *Geophys. Res. Lett.,* **35,** L08714, doi:10.1029/2008GL033317.

Raphael, M. N., and M. M. Holland, 2006: Twentieth century simulation of the Southern Hemisphere climate in coupled models. Part I: Large scale circulation variability. *Climate Dyn.,* **26,** 217–228.

Rayner, N. A., D. E. Parker, E. B. Horton, C. K. Folland, L. V. Alexander, D. P. Rowell, E. C. Kent, and A. Kaplan, 2003: Global analyses of sea surface temperature, sea ice, and night marine air temperature since the late nineteenth century. *J. Geophys. Res.,* **108,** 4407, doi:10.1029/2002JD002670.

Reason, C. J. C., and M. Rouault, 2005: Links between the Antarctic Oscillation and winter rainfall over western South Africa. *Geophys. Res. Lett.,* **32,** L07705, doi:10.1029/2005GL022419.

Renwick, J., and D. W. J. Thompson, 2006: The Southern Annular Mode and New Zealand climate. *Water Atmos.,* **14,** 24–25.

Reynolds, R. W., N. A. Rayner, T. M. Smith, D. C. Stokes, and W. Wang, 2002: An improved in situ and satellite SST analysis for climate. *J. Climate,* **15,** 1609–1625.

Russell, J. L., R. J. Stouffer, and K. W. Dixon, 2006: Intercomparison of the Southern Ocean circulations in IPCC coupled model control simulations. *J. Climate,* **19,** 4560–4575.

Screen, J. A., N. P. Gillett, D. P. Stevens, G. J. Marshall, and H. K. Roscoe, 2009: The role of eddies in the Southern Ocean

temperature response to the southern annular mode. *J. Climate,* **22,** 806–818.

Sen Gupta, A., and M. H. England, 2006: Coupled ocean–atmosphere–ice response to variations in the southern annular mode. *J. Climate,* **19,** 4457–4486.

Shi, G., J. Ribbe, W. Cai, and T. Cowan, 2008: An interpretation of Australian rainfall projections. *Geophys. Res. Lett.,* **35,** L02702, doi:10.1029/2007GL032436.

Shindell, D. T., and G. A. Schmidt, 2004: Southern Hemisphere climate response to ozone changes and greenhouse gas increases. *Geophys. Res. Lett.,* **31,** L18209, doi:10.1029/2004GL020724.

Silvestri, G. E., and C. S. Vera, 2003: Antarctic Oscillation signal on precipitation anomalies over southeastern South America. *Geophys. Res. Lett.,* **30,** 2115, doi:10.1029/2003GL018277.

Son, S.-W., and Coauthors, 2008: The impact of stratospheric ozone recovery on the Southern Hemisphere westerly jet. *Science,* **320,** 1486–1489.

Taylor, K. E., 2001: Summarizing multiple aspects of model performance in a single diagram. *J. Geophys. Res.,* **106,** 7183–7192.

Thompson, D. W. J., and J. M. Wallace, 2000: Annular modes in the extratropical circulation. Part I: Month-to-month variability. *J. Climate,* **13,** 1000–1016.

——, and S. Solomon, 2002: Interpretation of recent Southern Hemisphere climate change. *Science,* **296,** 895–899.

Turner, J., T. A. Lachlan-Cope, J. P. Thomas, and S. R. Colwell, 1995: The synoptic origins of precipitation over the Antarctic Peninsula. *Antarct. Sci.,* **7,** 327–337.

Uppala, S. M., and Coauthors, 2005: The ERA-40 Re-Analysis. *Quart. J. Roy. Meteor. Soc.,* **131,** 2961–3012.

van den Broeke, M. R., and N. P. M. van Lipzig, 2003: Response of wintertime Antarctic temperatures to the Antarctic Oscillation: Results of a regional climate model. *Antarctic Peninsula Climate Variability,* E. Domack et al., Eds., Antarctic Research Series, Vol. 79, Amer. Geophys. Union, 43–58.

Watterson, I. G., 2000: Southern midlatitude zonal wind vacillation and its interaction with the ocean in GCM simulations. *J. Climate,* **13,** 562–578.

——, 2007: Southern ''annular modes'' simulated by a climate model—Patterns, mechanisms, and uses. *J. Atmos. Sci.,* **64,** 3113–3131.

Xie, P., and P. A. Arkin, 1997: Global precipitation: A 17-year monthly analysis based on gauge observations, satellite estimates, and numerical model outputs. *Bull. Amer. Meteor. Soc.,* **78,** 2539–2558.